JOURNAL OF PROPULSION AND POWER
Vol. 15, No. 3, May–June 1999

Startup Modeling of the Receiver of NASA's 2-Kilowatt Solar Dynamic Power System

Guido W. Lopez*
Daniel Webster College, Nashua, New Hampshire 03063

A simplified approach to predict the thermal startup transient of the receiver of NASA's experimental 2-kW solar dynamic (SD) system, designed for the generation of power in space, is presented in this paper. This system is being tested at the NASA Lewis Research Center (NASA–LeRC) under low-Earth-orbit simulated conditions as part of the SD ground test demonstration program, which aims to address technology issues, develop experience, and validate theoretical models for future use of solar dynamic technology in space. One important technical issue being studied is the theoretical modeling of the transient-mode performance of SD systems, which has direct impact on off-design operation and control in an Earth-orbital environment. Preliminary correlation between experiment and existing theoretical predictions has suggested the need for improving existing models, such as the closed cycle engine program (CCEP), an in-house NASA computer code. Computational predictions based on the theoretical model presented in this paper show significant improvement in regard to startup receiver performance. To validate this model, comparisons between the experimental results obtained from the tests performed at the NASA–LeRC, and the computational predictions, are presented and discussed. The predictions of the simplified model show a close match with experimental results for values of solar energy near those reported in the experimental tests. Some predictions from the CCEP and pertinent discussion are also presented.

Introduction

SOLAR dynamic (SD) systems for power generation in space applications have been shown to have significant life-cost and launch mass benefits over conventional photovoltaic systems.[1] Theoretical and experimental research is underway to address technology issues and develop experience for future applications of SD power in space.[2–4,14] The 2-kW solar dynamic ground test demonstration (SD GTD), at NASA Lewis Research Center, (NASA–LeRC, now called John H. Glenn Research Center at Lewis Field), is a program whose main goal is to demonstrate system performance and collect data to support the use of SD technology for near- and long-term space application.[5–7]

Because SD power generation may represent a dramatic cut in the cost of large-scale power production in space (10 kW or more), several other efforts to further develop this technology are currently underway in the United States and Russia. Power production is an important part of space missions, and lower production costs represent substantial savings in the overall cost of a space mission. Ultimately, cost effectiveness of space systems facilitates the pursuance of new space programs.[15]

In addition to ongoing ground experimental work in tank-6 (see Fig. 1), at NASA–LeRC, and several analytical efforts to model the system, the United States and Russia have discussed plans to embark in a joint project of flight demonstration of SD power generation in space.[8] This is an initiative from the International Space Station Program Office, and its goal is to demonstrate the capability of SD systems during orbital space flight. The analytical and experimental results of these projects carry considerable potential for application in the power production system of the International Space Station Alpha, and in future solar-power generation for communication satellites.

One important technical issue of SD systems modeling is the transient mode performance that has a direct impact on off-design operation and control of the system for applications in an Earth orbital environment. Several codes have been used to model and simulate orbital startup and shutdown transients.[9–11] Preliminary correlation between experimental and analytical results from these codes suggests the need to improve the analytical models to better reflect the experimental results. The experimental results that are being obtained from tests on the SD GTD at NASA–LeRC are an invaluable reference to better understand the parameters involved, and characteristics of the transient system performance.[5,12,13] The SD GTD program of tests is well under way, and the results from the experiments performed in tank-6 at NASA–LeRC for simulated orbital conditions are the fundamental bases for model validation.

A simplified approach to model the startup transient of the receiver of the SD system is presented in this paper. The results of the analytic model are compared with experimental data obtained from the tests performed at NASA–LeRC. Validation of the model and future recommendations are discussed.

General Characteristics of the SD System's Receiver

The receiver of the SD system (see Fig. 2) consists of a cylindrical metal cavity inside which there is a number of tubes evenly and circumferentially distributed, at a short distance with respect to the inside face of the cavity. There are cylindrical canisters stacked along the length of the tubes. These canisters contain a mixture of Li F and CaF_2, the phase change material (PCM), which stores the energy required to operate the system during eclipse periods. The tubes are connected to input and output manifolds enclosed in subcavities in front and in back of the receiver. There is a conical aperture attached to the cylindrical cavity. The circular opening of the cone has a small offset with respect to the axis of the cylindrical cavity. The receiver is insulated at the sides, back, and front. In addition, the front of the receiver is shielded to prevent the melting of the wall metal.

General Description of the Receiver Startup Operation

Solar energy is reflected and focused by a concentrator onto the aperture of the receiver. The focal point of the concentrator is just inside the aperture of the receiver. The energy eventually strikes the canisters and the inside walls of the cavity. A complicated pattern of energy reflections in the cavity occurs. Part of the energy will be reflected back to the aperture and then lost. Another part of the energy will be lost by conduction, through the walls and insulation of the cavity, and the remaining energy will be conducted and convected to the PCM and to the working fluid (a xenon–helium gas mixture) in the tubes. Under suitable steady operating conditions, the working fluid carries the energy to the turbine-generator system for transformation.

Received April 20, 1998; revision received Aug. 24, 1998; accepted for publication Aug. 26, 1998.

*Chairperson, Engineering Division, 20 University Drive; lopez@dwc.edu.

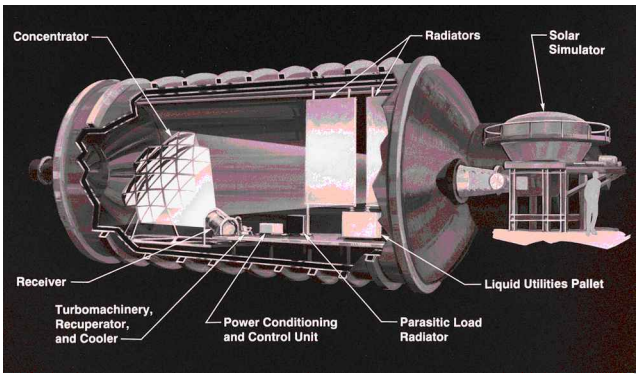

Fig. 1 SD GTD.

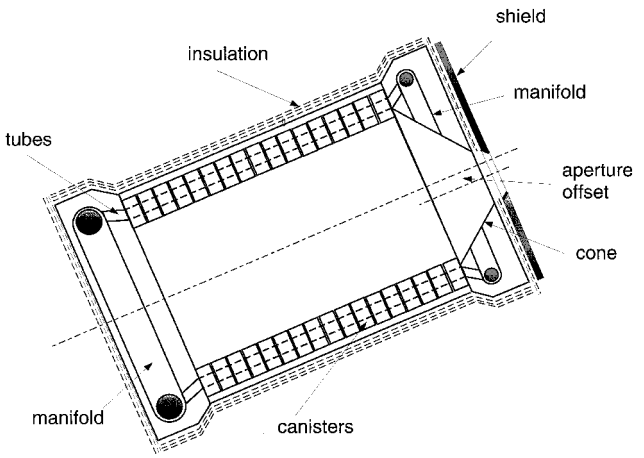

Fig. 2 Schematic longitudinal cut of the SD Brayton system receiver.

Under startup conditions, the operation of the receiver is as follows: initially, all of the elements of the receiver and the working fluid are at a uniform temperature T_0. The working is initially trapped in the tubes and manifolds. The gas is not allowed to circulate until after predetermined pressure and temperature conditions are reached, as a result of the transient heating in the cavity. The PCM is initially in the solid phase.

There is a sudden input of solar energy through the aperture of the cavity, and the temperatures of the elements of the receiver rise as a function of time. The energy reaching the canisters penetrates their wall by conduction reaching the solid PCM, and eventually, the trapped working fluid. Sensible heating of the PCM exists until its temperature reaches the melting point. The melting process is not expected to be uniform as a result of the irregular distribution of substance in the canisters, and as a result of the presence of voids in the solid phase, which are intended to compensate for the increase in volume during the change to the liquid phase. Furthermore, the incident energy on the canisters is not uniform, as a result of the complicated pattern of energy reflections in the interior of the cavity.

There is also transfer of energy into and out of the subcavities containing the manifolds. Some energy is conducted and convected by the fluid in the canister region, and some energy is radiated and reflected from the walls of these subcavities. There is also heat loss through the external insulated walls of these subcavities. The overall effect, however, is the heating of the working fluid in the manifolds. The motion of the fluid is controlled by valves that are opened when the wall temperature of a predetermined canister reaches a predetermined temperature, whose value is slightly higher than the melting point of the PCM. Ideally, all of the PCM in all canisters will be melted at this moment.

System Simplification for Development of an Analytical Transient Model of the Receiver

Fundamental thermal analysis is developed by subdividing the receiver into simplified subelements. The following subelements are identified: 1) front manifold subcavity, 2) cylinder–cone subcavity (side and back walls and cone of cavity), and 3) back manifold subcavity.

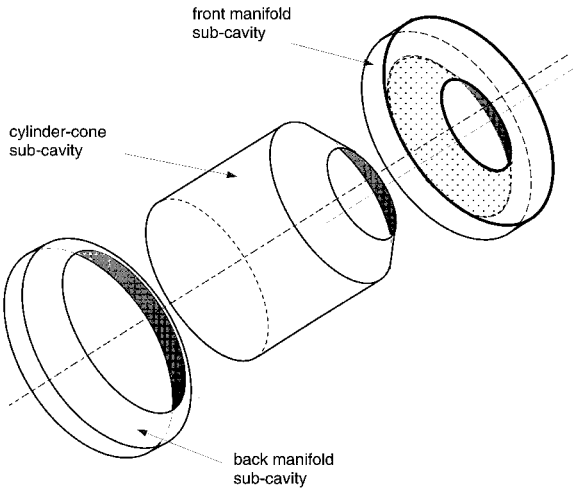

Fig. 3 Exploded view of the subcavities of the SD Brayton system receiver.

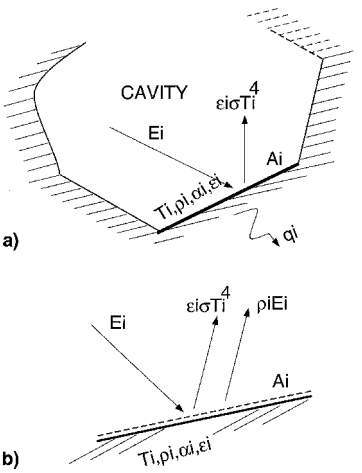

Fig. 4 Energy parameters of surface A_i of a cavity.

An exploded view of these subelements of the system is presented in Fig. 3. The cylinder–cone subcavity is exclusively designed to capture solar energy for transmission and storage. Therefore, the radiative analysis of this subcavity is of particular interest for the development of the receiver analytical model.

Thermal Radiation Analysis of the Cylinder–Cone Subcavity: Fundamental Theory

The purpose of the cylinder–cone subcavity of the receiver is to efficiently trap and store the solar radiation incident in it. The following radiation heat transfer analysis is the first step toward the development of the analytic model of the receiver.

Consider the surface A_i of a cavity, as represented in Fig. 4a. In this figure, E_i, ε_i, α_i, and ρ_i represent the incident hemispherical emissive power, emittance, absorptance, and reflectance associated with the surface, respectively. The net amount of energy that could eventually be transferred by conduction into the walls of the system is

$$(Q/A) = q_i = \alpha_i E_i - \varepsilon_i \sigma T_i^4 \tag{1}$$

The radiosity R_i of the surface A_i (see Fig. 4b) is

$$R_i = \varepsilon_i \sigma T_i^4 + \rho_i E_i \tag{2}$$

Note that incident energy on a surface A_i in a cavity is the sum of all radiosities of the cavity's surfaces, including itself (it will be zero if the surface is perfectly flat). Therefore

$$A_i E_i = \sum_{j=1}^{M} R_j A_j F_{j-i} = \sum_{j=1}^{M} R_j A_i F_{i-j} \tag{3}$$

where $i = 1, 2, 3, \ldots, M$; $j = 1, 2, 3, \ldots, M$; and $M =$ number of surfaces of cavity.

The terms F_{j-i} and F_{i-j} of this equation represent the fraction of the radiosity from surface j that reaches surface i and vice versa, respectively.

The terms F_{j-i} and F_{i-j} are commonly referred to as the configuration factors and are entirely dependent on the geometry and orientation of the surfaces. Then, from Eqs. (1–3)

$$q_i = \sum_{j=1}^{M} R_j F_{i-j} - R_i \tag{4}$$

taking the term $i = j$ out of the summation expression, and simplifying, we have

$$q_i = R_i(F_{i-i} - 1) + \sum_{j=1}^{M} R_j F_{i-j} \tag{5}$$

This equation can be used to evaluate radiosities of the surfaces in cavities where the q_i are known. The sum term is applicable for $i \neq j$.

On the other hand, if the temperature of the surfaces of the cavity are known, the following expression can be derived by combining Eqs. (2) and (3):

$$q_i = [(1-\varepsilon_i)F_{i-i} - 1]R_i + (1-\varepsilon_i)\sum_{j=1}^{M} R_j F_{i-j} = -\varepsilon_i \sigma T_i^4 \tag{6}$$

where the summation term is applicable for all i and j, such that $i \neq j$.

Analysis of Cavity with an Aperture and External Radiative Energy

Consider the cavity shown in Fig. 5a. The energy Ep is continuously flowing into the cavity through aperture A_1. This energy will eventually reach the surfaces of the cavity, and undergo absorption and reflection. The amount of energy that returns to the aperture as a result of the emission and reflection in the surfaces of the cavity is

$$Q_{\text{returning}} = \sum_{i=2}^{M} R_j A_i F_{i-1} \tag{7}$$

Therefore, the net amount of energy transferred to the cavity is

$$Q_{\text{net}} = E_p A_1 - \sum_{i=2}^{M} R_i F_{i-1} A_i = A_1 \left(E_p - \sum_{i=2}^{M} R_i F_{1-i} \right) \tag{8}$$

Assuming that the external energy Ep, entering the aperture, is uniformly diffused in all directions, the incident energy on a surface A_i of the cavity is the sum of the energies coming from the other surfaces of the cavity and the fraction of Ep coming from the aperture A_1 (see Fig. 5b). Thus

$$A_i E_i = E_p A_1 F_{1-i} + \sum_{j=2}^{M} R_j A_j F_{j-i}$$

$$= A_i \left(E_p F_{i-1} + \sum_{j=2}^{M} R_j F_{i-j} \right) \qquad i = 2, 3, 4, \ldots, M \tag{9}$$

Therefore, the radiosity of the surface A_i can be written as follows:

$$A_i R_i = \rho_i A_i \left(E_p F_{i-1} + \sum_{j=2}^{M} R_j F_{i-j} \right) + A_i \varepsilon_i \sigma T_i^4$$

$$i = 2, 3, 4, \ldots, M \tag{10}$$

This expression can also be written as follows:

$$\left[F_{i-i} - \frac{1}{(1-\varepsilon_i)} \right] R_i + \sum_{j=2}^{M} R_j F_{i-j}$$

$$= -\left[E_p F_{i-1} + \frac{\varepsilon_i}{(1-\varepsilon_i)} \varepsilon_i \sigma T_i^4 \right]$$

$$i = 2, 3, 4, \ldots, M \tag{11}$$

where the sum term is valid for $i \neq j$, and the radiosity fraction of element i, incident onto itself, now appears in the first bracket instead of the sum term. This equation can be used to find the radiosities of all surfaces in the cavity, provided that the temperatures and magnitude of the external incident energy Ep are known, in addition to the geometry of the cavity. The evaluation of the F_{i-j} is done based on view factor algebra as explained in the next section.

Evaluation of View Factors for the Receiver Cylinder–Cone Subcavity

The cylinder–cone subcavity is modeled by considering the following surfaces (see Fig. 6): surface 1 = aperture; surface 2 = cone side; surface 3 = back circular surface; and surfaces 4, 5, 6, ..., M = side cylindrical surfaces.

The side surfaces, 4, 5, 6, ..., M, are subdivisions of the cylindrical side of the cavity. The number of these subdivisions depends on the accuracy required. These surfaces are of equal area. Fictitious circular surfaces $a_0, a_1, a_2, a_3, \ldots, a_M$, are used for the analysis and evaluation of view factors. These areas are concentric and parallel to each other. Figure 6 shows details of the geometry used for the analysis. Through view factors algebra,[16] the evaluation of view factors among the surfaces of the receiver can be simplified to expressions that ultimately involve only the calculation of the view factor between two flat–concentric parallel disks, as shown in Fig. 7. This expression is

$$F_{a-b} = \tfrac{1}{2}\left[X - \sqrt{X^2 - 4(R_2/R_1)^2} \right] \tag{12}$$

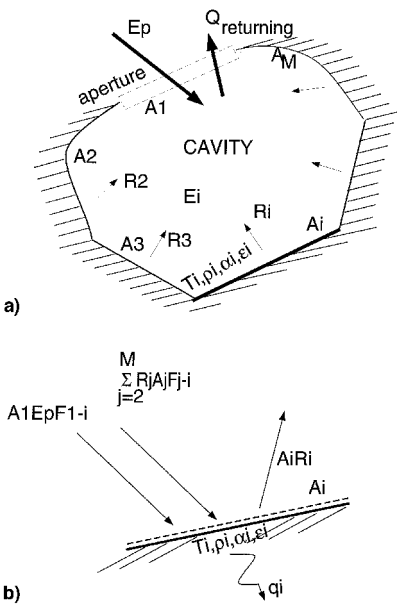

Fig. 5 Radiation exchange in a cavity with aperture *A*1 and external incident energy *Ep*.

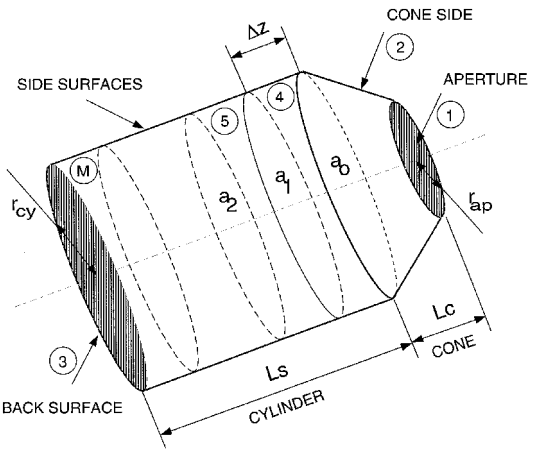

Fig. 6 Receiver cavity geometry for view factor evaluation.

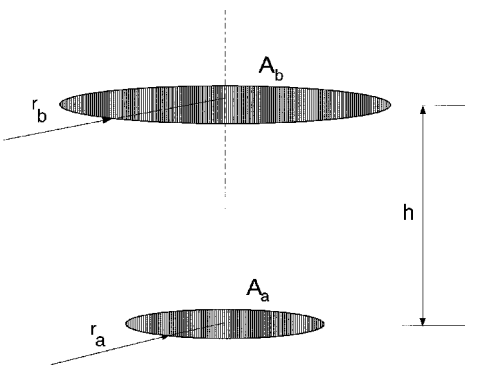

Fig. 7 Geometry of two concentric–parallel disks for view factor evaluation.

where

$$R_1 = r_a/h, \qquad R_2 = r_b/h, \qquad X = 1 + \left[\left(1 + R_2^2\right)/R_1^2\right]$$

When using these equations, the radii r_a and r_b, and the height h, are related to the geometry of the cavity determined by the configuration of pairs of surfaces. Mathematical expressions for view factors between two surfaces are developed using techniques of view factors algebra. The following sections present an expanded development of view factor calculation for the surfaces of the cavity.

View Factors Relative to Surface 1

The view factor F_{1-1} is zero because the aperture is modeled as a flat disk.

F_{1-2} is calculated from the equation

$$F_{1-2} = 1 - F_{1-a0} \tag{13}$$

F_{1-3} can be calculated directly from Eq. (12), where r_a is the radius of aperture r_{ap}, r_b is the radius of cavity cylinder r_{cy}, and h is the $Lc + Ls$ (height of cone plus height of cylinder).

The view factors F_{1-j} for $j \geq 4$ are calculated from

$$F_{1-j} = F_{1-a(j-4)} - F_{1-a(j-3)} \tag{14}$$

In general, the F_{1-ak} are disk-to-disk view factors that can be evaluated from Eq. (12), where h is $Lc + k\Delta z$ (see Fig. 6), where $k = 0, 1, 2, \ldots$.

View Factors Relative to Surface 2

F_{2-1} is calculated from

$$F_{2-1} = (A_1/A_2)F_{1-2} \tag{15}$$

F_{2-2} is evaluated from

$$F_{2-2} = [1 - (A_0/A_2)] + (A_1/A_2)(2F_{1-a0} - 1) \tag{16}$$

where

$$A_0 = \pi r_{cy}^2, \qquad A_1 = \pi r_{ap}^2$$

$$A_2 = \pi(r_{ap} + r_{cy})\sqrt{L_c^2 + (r_{cy} - r_{ap})^2}$$

For view factor F_{2-3} we have

$$F_{2-3} = (A_0/A_2)F_{a0-3} - (A_1/A_2)F_{1-3} \tag{17}$$

The expression for calculating F_{2-4} is

$$F_{2-4} = (A_0/A_2)(1 - F_{a0-a1}) - (A_1/A_2)(F_{1-a0} - F_{1-a1}) \tag{18}$$

The following general expression can be used for view factors F_{2-j}, where $j \geq 5$:

$$F_{2-j} = (A_0/A_2)\left[F_{a0-a(j-4)} - F_{a0-a(j-3)}\right] - (A_1/A_2)\left[F_{1-a(j-4)} - F_{1-a(j-3)}\right] \tag{19}$$

All view factors on the right-hand side (RHS) of the last two equations can be evaluated from the disk-to-disk view factor [Eq. (12)]. The calculation of the F_{1-ak} was explained in the previous section. The calculation of the view factors F_{a0-ak}, where $k = 1, 2, 3, \ldots, M$, is explained in the section relative to surface i, when $i \geq 4$.

View Factors Relative to Surface 3

Based on previously calculated view factors, we have

$$F_{3-1} = (A_1/A_3)F_{1-3} \tag{20}$$

$$F_{3-2} = (A_2/A_3)F_{2-3} \tag{21}$$

$$F_{3-3} = 0 \tag{22}$$

For $j \geq 4$, a general expression can be developed for the view factors F_{3-j}, such that

$$F_{3-j} = F_{3-a(j-3)} - F_{3-a(j-4)} \tag{23}$$

The view factors on the RHS of this equation can be readily calculated from the disk-to-disk expression [Eq. (12)]. The following applies when calculating the F_{3-ak} using Eq. (12): $r_a = r_b = r_{cy}$, and $h = Ls - k\Delta z$ (see Fig. 6).

View Factors Relative to Surface *i*, Where $i \geq 4$

General expressions for view factors F_{i-j}, where $i \geq 4$ and $j = 1, 2, 3, \ldots, M$, can be readily developed making use of view factor algebra. A summary of these equations is presented next.

Case a, $i \geq 4$ and $j < i$:

$$F_{i-j} = (A_j/A_i)F_{j-i} \tag{24}$$

Case b, $i \geq 4$ and $j \geq i$:

Subcase b1, $j = i$:

$$F_{i-j} = 1 - 2(A_0/A_i)\left[1 - F_{a(i-4)-a(j-3)}\right] \tag{25}$$

Subcase b2, $j = i + 1$:

$$F_{i-j} = (A_0/A_i)\left\{\left[1 - F_{a(i-3)-a(j-3)}\right] - \left[F_{a(i-4)-a(j-4)} - F_{a(i-4)-a(j-3)}\right]\right\} \tag{26}$$

Subcase b3, $j \geq i + 2$:

$$F_{i-N} = (A_0/A_i)\left\{\left[F_{a(i-3)-a(j-4)} - F_{a(i-3)-a(j-3)}\right] - \left[F_{a(i-4)-a(j-4)} - F_{a(i-4)-a(j-3)}\right]\right\} \tag{27}$$

in all of these cases: $i = 4, 5, 6, 7, \ldots, M$; $j = 1, 2, 3, 4, \ldots, M$; $A_i = 2\pi r_{cy}\Delta z$; and $A_0 = \pi r_{cy}^2$.

The $F_{a_l - a_k}$ are view factors between disks of the same diameter, but at different distances from each other. With the exception of F_{a0-a0}, which is the view factor of area $a0$ in reference to itself ($a0$ is a flat disk surface, therefore F_{a0-a0} is zero), the view factors $F_{a_l - a_k}$ can be recalculated from the general disk-to-disk view factor equation as presented next:

$$F_{a_l - a_k} = \tfrac{1}{2}\left[X_{lk} - \sqrt{X_{lk}^2 - 4\left(R_{2_{lk}} / R_{1_{lk}}\right)^2}\right] \tag{28}$$

where

$$R_{1_{lk}} = R_{2_{lk}} = r_{cy}/h_{lk}, \qquad X_{lk} = 1 + \left[\left(1 + R_{2_{lk}}^2\right)/R_{1_{lk}}^2\right]$$

$$h_{lk} = (k - l)\Delta z, \quad \text{for} \quad k \neq l$$

Simplified Transient Model of the Elements of the Cylinder–Cone Subcavity

The elements of the cavity, i.e., pipes, canisters, PCM, and walls, are intimately associated to the surfaces used for the radiation exchange analysis. A simplified transient analysis of these elements can be developed using the lumped parameter system approach as follows. For an element i of the subcavity

$$m_i c_i \frac{dT_i(\upsilon)}{d\upsilon} = Q_i(\upsilon, T) \tag{29}$$

where m_i = mass of element, c_i = specific heat, υ = time, T_i = temperature, and Q_i = incoming energy.

Note that Q_i is a function of both time and temperature. A discrete approach can be used to solve this equation. The solution can be obtained implicitly or explicitly as follows.

Implicit:

$$T_i^{n+1} - (\Delta\upsilon/m_i c_i)Q_i^{n+1} = T_i^n \tag{30}$$

Explicit:

$$T_i^{n+1} = (\Delta\upsilon/m_i c_i)Q_i^n + T_i^n \tag{31}$$

The net amount of energy Q_i is obtained from the analysis of radiation heat input and heat losses to the environment (space equivalent temperature T_{env}). In general

$$Q_i(\upsilon, T) = Q_{\text{input by radiation}} - Q_{\text{loss}} \tag{32}$$

Through thermocircuit analysis, the heat losses can be evaluated from

$$Q_{\text{loss}} = [T_i(\upsilon) - T_{env}]/R_T \tag{33}$$

where R_T is the total thermal resistance corresponding to the temperature potential $T_i(\upsilon) - T_{env}$. This resistance depends on geometry and properties of the various elements of the subcavities of the receiver. For example, the thermal resistance R_T through the composite walls of cylindrical elements takes into account the thicknesses and thermoconductivities (shown next) of the inner liner, the metallic skin (Haynes 188), and the multifoil (blankets of nickel and aluminum) insulation (MLI), wrapped around the metallic skin, and because the MLI faces the surrounding space, the R_T also depends on the effective emissivity of this material. Important receiver data: sun power at the aperture = 12.5, 11.5, 10 kW; initial soak temperature = 311 K (560°R); sun period = 66 min; eclipse period = 27 min; melting point of PCM = 1041 K (1872.7°R); total mass of PCM = 24 kg (53 lbm); radius of aperture = 88.9 mm (3.5 in.); radius of optical control surface (OCS) = 241.3 mm (9.5 in.); total length cavity = 762 mm (30 in.); canister per pipe = 24; outside radius of canister = 27.7 mm (0.895 in.); canister width = 25.4 mm (1.0 in.); pipes o.d. = 22.225 mm (0.875 in.); inlet manifold o.d. = 50.8 mm (2.0 in.); outlet manifold o.d. = 86.36 mm (3.4 in.); liner thickness = 12.7 mm (0.5 in.); thickness of insulation = 19.05 mm (0.75 in.); time increment = 1 min; liner thermoconductivity = 10 Kcal/m h °C; thermoconductivity of Haynes 188 = 15.6 W/m K; effective thermoconductivity of MLI = 5.2 W/m K; MLI effective emissivity = 0.1; density of Haynes 188 = 9130.5 kg/m^3 (570 lbm/ft^3); specific heat of PCM = 1.775 kJ/kg K (0.424 Btu/lbm °F); specific heat of Haynes 188 = 535.9 J/kg K (0.128 Btu/lbm °F). In this particular case, the total thermal resistance can be evaluated from the expression

$$R_T = \frac{1}{A_i}\left[\left(\frac{t}{k}\right)_{\text{liner}} + \left(\frac{t}{k}\right)_{\text{metal skin}} + \left(\frac{t}{k}\right)_{\text{MLI}} + \left(\frac{1}{4\varepsilon\sigma T_{env}^3}\right)\right] \tag{34}$$

where t represents the thickness, k is the thermal conductivity, σ is the Stefan–Boltzmann constant, and ε is the effective thermal emissivity of the MLI. For the cylindrical elements, therefore, Q_{loss} is first conducted through the layers of the composite wall and ultimately radiated to the surrounding space at an effective temperature, T_{env}.

The results from Eqs. (30) and (31) represent the temperature variation with respect to time of the elements of the receiver. Validation of the model is done using temperature variation of the receiver canisters.

Computer Simulation: Conditions and Results

A computer code (SIMPLECode) written in Fortran 77, was developed to simulate startup operation of the receiver based on the mathematical model explained in the previous sections. A general flow diagram of this code is presented in Fig. 8. The data required to run the program for temperature prediction of startup operation was directly taken from the experimental unit installed in tank-6 at NASA–LeRC (see Fig. 9). These data include geometry, transport, and thermodynamic properties of materials, and conditions of experimentation. It should be emphasized that thermophysical properties depend on temperature level. This dependency, however, was not taken into consideration for the model computations.

The reference experiments for comparison and discussion are taken from the tests performed by the SD GTD team on April 3 and 4, 1995, and the one performed one year later on April 4, 1996, at the NASA–LeRC.[†] These tests are two in a series of experiments of

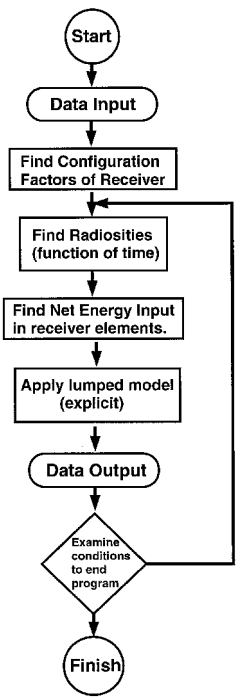

Fig. 8 Flow diagram of computer simulation code.

[†]Mason, L., "SD GTD Test Report #4," and Report of April 4, 1996, NASA–LeRC, Cleveland, OH.

the SD GTD program, whose main objective is to develop further experience on SD performance for space applications and model validation. The most important data used to run the computerized model and the experiment are summarized in the previous text.

The computer code calculates the variation of the canister temperatures at different locations within the receiver cavity as a function of time. The average canister temperature in the cavity is then evaluated and compared with the experimental average canister temperature from the tests in tank-6. Graphical comparisons of experimental and theoretical results are presented in Figs. 10 and 11. Each figure shows the experimental and theoretically predicted average canister temperature as a function of time for startup conditions.

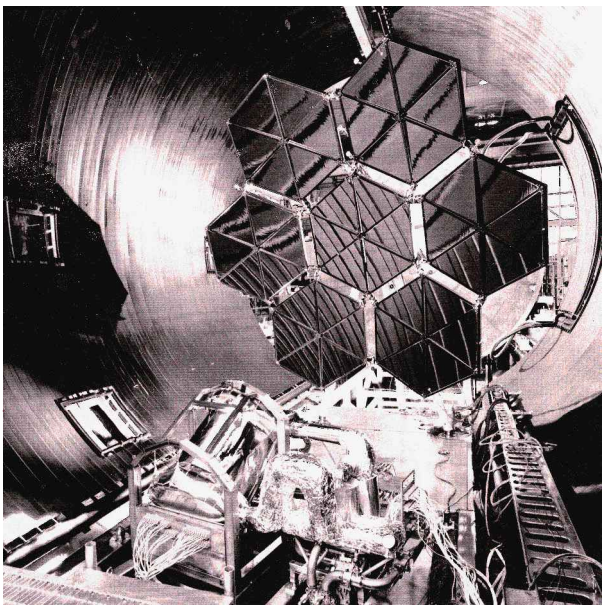

Fig. 9 SD system installed in tank 6 at NASA–LeRC.

CCEP Code and Its Computer Simulation Results

The closed cycle engine program (CCEP) is an in-house NASA–LeRC computer code that has been developed to analyze and simulate performance of closed-cycle Brayton space systems for power generation in space. It evolved in the early 1980s and it has its roots in the Navy/NASA engine program, developed for the simulation and design of aircraft gas-engine systems. The CCEP program is currently being tested against experimental data from the SD GTD program. Preliminary correlation between the CCEP prediction of startup operation of the receiver and actual experimental data is being analyzed at NASA–LeRC. A case comparison between experimental data and predictions from the CCEP program is presented in Fig. 12, for three levels of solar power at the aperture of the receiver. This comparison is in reference to the SD GTD test of April 4, 1995 used in the comparison of Fig. 10.

Discussion of Results

The immediate availability of data from the actual system being tested at NASA–LeRC constitutes one of the advantages of the development of the simplified model presented in this paper, over models that have been developed prior to the design, construction, and testing of an actual experimental unit, such as the CCEP code. Direct observations of the tests' characteristics and geometry of the SD unit were instrumental for conceptualizing the analytical model, and they greatly facilitated the choice of simplifications and assumptions.

In general, the comparison presented in Figs. 10 and 11 shows a close qualitative and quantitative correlation between the theoretical predictions of the simplified model and experimental results. The

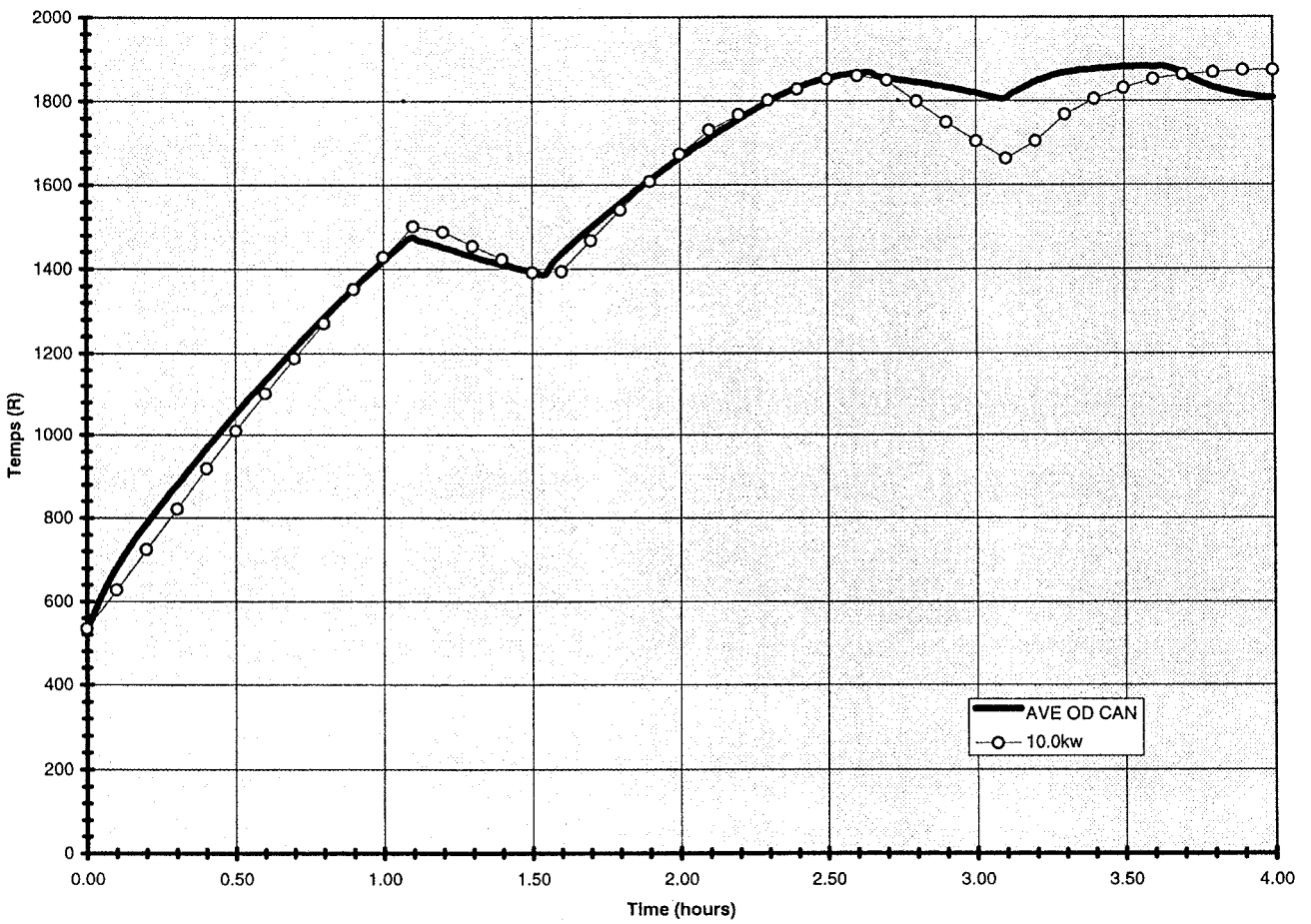

Fig. 10 Comparison between experimental and simulated mean canister temperature. Test of April 1995 (solar power input = 10.0 kW).

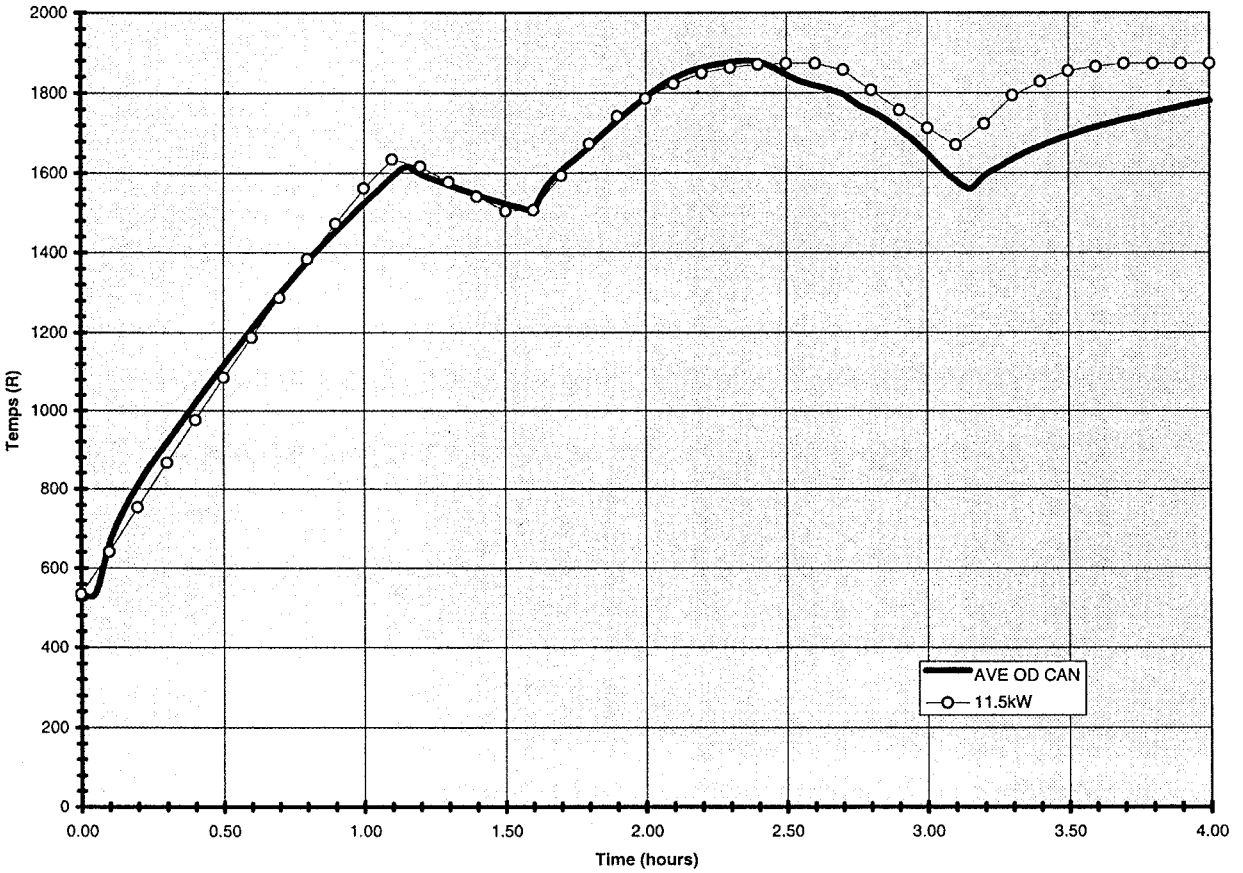

Fig. 11 Comparison between experimental and simulated mean canister temperature. Test of April 1996 (solar power input = 11.5 kW).

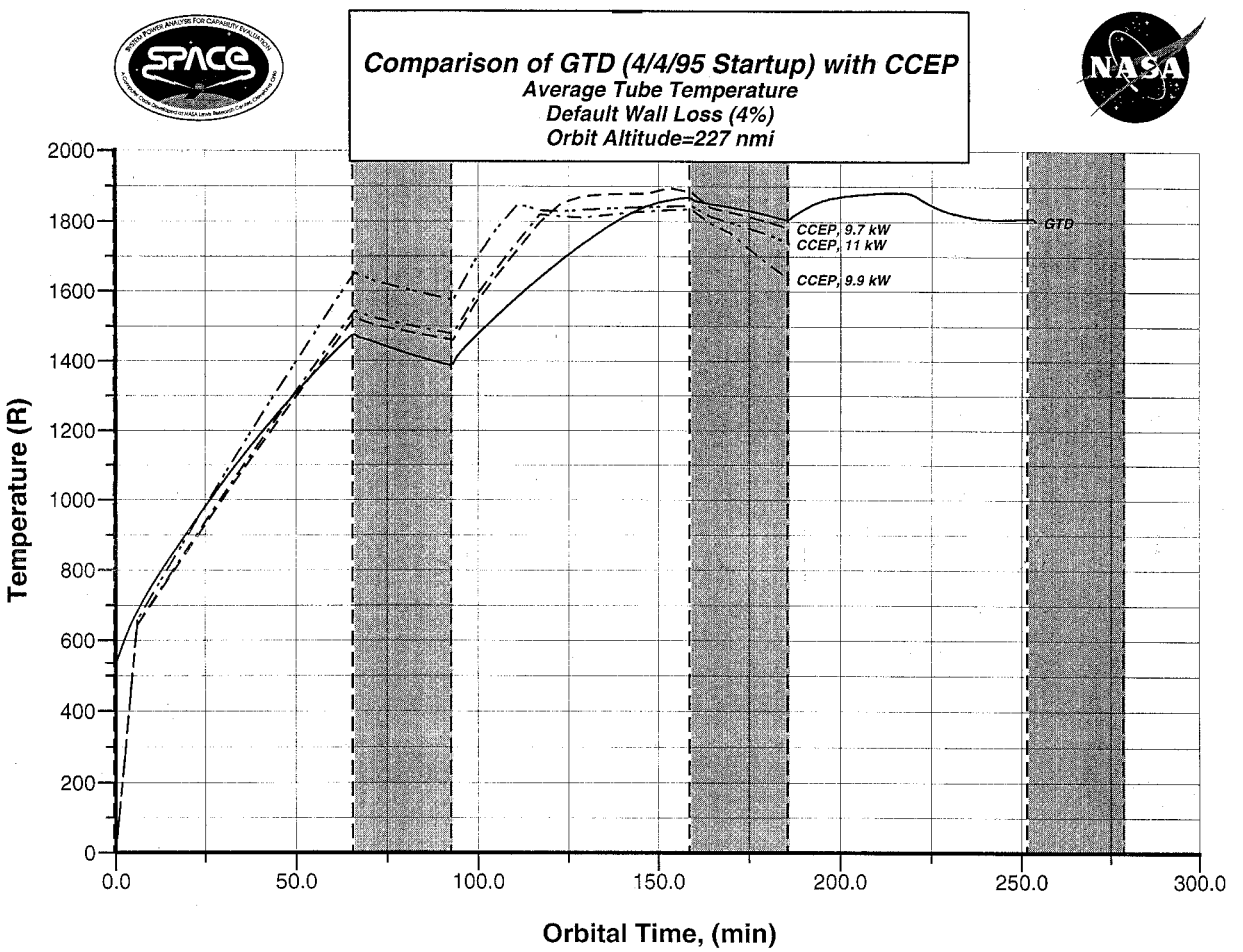

Fig. 12 Comparison between experimental and simulated mean canister temperature. CCEP code. Test of April 1995.

value of the incident solar power at the aperture of the receiver is an important part of the input data of the program. The closest agreement between theory and experience is obtained when this power input is selected at 10 and 11.5 kW for the cases studied. There have been several efforts to accurately measure the incident radiation at the aperture. However, there still exists some uncertainty among the experimentalist at NASA–LeRC, regarding the measurement of the level of the effective solar power entering the aperture of the receiver. The results from the computer simulations suggest that the selected insolation levels of 10 and 11.5 kW can be considered accurate.

Computer predictions using other values of insolation consistently show noticeable or substantial discrepancy, when compared with the experimental temperature values, particularly at the beginning of the first eclipse (points around 1 h). The reported experimental values of solar power entering the aperture at startup conditions are 9.64 kW for the April 1995 test, and 11.7 kW for the April 1996 test. The percent difference between the values used in the model and those reported from experiment are 3.67 and 1.72% for April 1995 and April 1996, respectively.

Discrepancy between model prediction and experiment is observed in all trials for times beyond the point where the average canister temperature first reaches the melting point of the PCM, 1040.4 K (1872.7°R). There is a simple explanation for this discrepancy. The simplified model was not designed to model the melting process (latent behavior) of the PCM in the canisters. The theoretical model only predicts sensible heating behavior of the elements of the receiver, including the PCM contained in the canisters. The domain of the theoretical prediction ranges between the initial temperature and the initiation of the melting process of the PCM in the canisters.

Also, a more detailed examination of the curves indicates a small but consistent discrepancy within the eclipse period of the orbit. It may be concluded that the time response of the model does not match exactly that of the experimental unit. Given the number of variables involved in the computational model, this small discrepancy is to be expected. It suggests, however, a closer revision of values of geometric and thermal properties used in the computations, because these parameters directly affect the time response of the theoretical model (in purely lumped systems, this is identified as the time constant of the system).

The results from the CCEP are also presented for comparison. Three levels of insolation were used: 9.7, 9.9, and 11.0 kW. The graphical results from this code clearly suggest the need to review or change the model used in the CCEP code, to simulate startup operation of the receiver. The discrepancy between experiment and model from the CCEP code is evident for all levels of insolation used in the comparison.

Summary

The startup operation of NASA's 2-kW SD power system has been modeled using a simple but effective mathematical approach. Results from the simplified model presented in this paper are in close agreement with results obtained from tests at NASA-LeRC. On the basis of this agreement, it may be concluded that the values of insolation used for the computations are an accurate theoretical estimate of the actual insolation at the aperture of the receiver. The results are highly satisfactory, and there is potential for further enhancement. This model, for example, can be modified and adapted to include system behavior beyond the melting point of the PCM in the canisters.

Acknowledgments

The author wishes to thank all members of the NASA–LeRC SD GTD project team. Without their help and cooperation, the development and validation of this model would not have been possible. Special thanks to Richard Shaltens, the SD GTD Project Manager, and team members Lee Mason and Frank Madi.

References

[1]Connelly, D. R., "Flexibility of the Closed Brayton Cycle for Space Power," AlliedSignal Aerospace Co., TP# AS 41-8443, Tempe, AZ, Dec. 1988.

[2]Howell, J., "Technical Proposal for the 2 kW Solar Dynamic Space Power System Ground Test Demonstration," AlliedSignal Aerospace Co., AS 41-10919-2, Tempe, AZ, Feb. 1992.

[3]Kesseli, J., Saunders, R., and Batchelder, G., "The Advanced Heat Receiver Conceptual Design Study," NASA CR-182177, Oct. 1988.

[4]Tolbert, C., "Selection of Solar Simulator of Solar Dynamic Ground Test," NASA TM-106608, Aug. 1994.

[5]Shaltens, R., "Overview of the Solar Dynamic Ground Test Demonstration Program at the NASA Lewis Research Center," NASA TM-106296, Aug. 1993.

[6]Jefferies, K., "Solar Simulator for Solar Dynamic Space Power System Testing," NASA TM-106393, Aug. 1994.

[7]Mock, T., "Solar Dynamic Ground Test Demonstrator (SDGTD). System Thermodynamic Integration Results from PDR Plus Continuous vs. Orbital System Operation," AlliedSignal Aerospace Co., AS 41-111611, Tempe, AZ, Dec. 1992.

[8]Kerslake, T., and Fincannon, J., "Analysis of Solar Receiver Flux Distribution for US/Russian Solar Dynamics System Demonstration on the MIR Space Station," NASA TM-106933, July 1995.

[9]Mock, T., "SDGTD (Solar Dynamic Ground Test Demonstrator) Computer Model DEMO," AlliedSignal Aerospace Co., AS 41-12408, Tempe, AZ, Oct. 1993.

[10]Klan, J., "Closed Cycle Engine Program (CCEP)," Reference Information, NASA Lewis Research Center, Cleveland, OH, Sept. 1993.

[11]Skarda, J., "Thermal Modeling with Solid/Liquid Phase Change of the Thermal Energy Storage Experiment," NASA TM-103770, Nov. 1991.

[12]Boyle, R., "Fourth Monthly Technical/Schedule Status Report for the NASA–LeRC Solar Dynamic Ground Test Demonstration (SD GTD)," Allied Signal Aerospace Co., AS 41-11367-I(4), Tempe, AZ, Aug. 1992.

[13]Shaltens, R., and Boyle, R., "Initial Results from the Solar Dynamics (SD) Ground Test Demonstration (GTD) Project at NASA Lewis," NASA TM-107004, July 1995.

[14]Knuston, K., "Uncertainty Analysis for the Data Acquisition and Control Subsystem of the Solar Dynamic Ground Test Demonstration (SDGTD)," AlliedSignal Aerospace Co., AS 41-12088, Tempe, AZ, May 1993.

[15]Brandhorst, H., "Space Power, What Is Old Is New Again," AIAA-94-3784, 1994.

[16]Mills, A. F., "Radiation Exchange Between Surfaces," *Heat Transfer*, 1st ed., Irwin, Homewood, IL, 1992, pp. 496–503.